Supporting Information

Targeted synthesis and reaction mechanism discussion of Mo_2C based insertion-type electrodes for advanced pseudocapacitors

Yuanyuan Zhu†[a, e], Xu Ji†[b], Lufeng Yang[c], Jin Jia[d], Shuang Cheng[a,*], Hailong Chen[c], Zhong-Shuai Wu[e], Donata Passarello[f] and Meilin Liu[g]

[a] New Energy Research Institute, School of Environment and Energy, South China University of Technology, Guangzhou, 510006, People's Republic of China.

[b] College of Automation, Zhongkai University of Agriculture and Engineering, Guangzhou, 510225, People's Republic of China

[c] The Woodruff School of Mechanical Engineering, Georgia Institute of Technology, 771 Ferst Drive, Atlanta, GA 30332-0245, USA.

[d] Institute for Advanced Interdisciplinary Research, Collaborative Innovation Center of Technology and Equipment for Biological Diagnosis and Therapy in Universities of Shandong, University of Jinan, Jinan 250011, People's Republic of China.

[e] Dalian National Laboratory for Clean Energy, Dalian Institute of Chemical Physics, Chinese Academy of Sciences, 457 Zhongshan Road, Dalian 116023, People's Republic of China.

[f] Stanford Synchrotron Radiation Lightsource, SLAC National Accelerator Laboratory, Menlo Park, CA, USA

[g] School of Materials Science and Engineering, Georgia Institute of Technology, Atlanta, GA 30332-0245, USA.

† Yuanyuan Zhu and Xu Ji contributed equally to this work.

* Corresponding author. E-mail address: escheng@scut.edu.cn (S. Cheng).

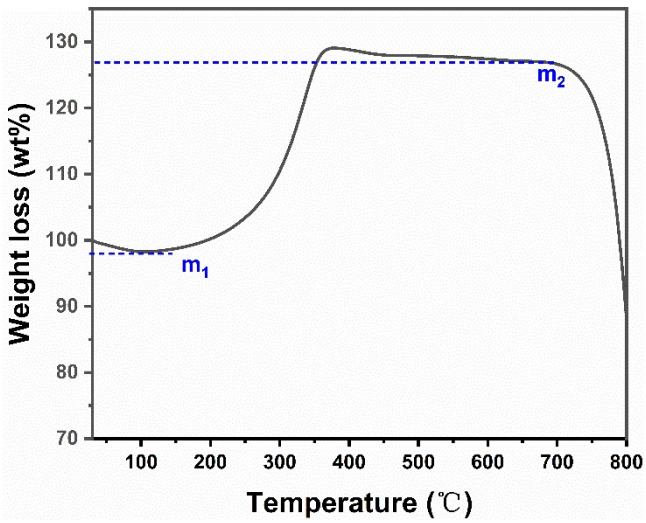

Fig. S1 TGA curve of the as-prepared N-Mo_2C/C sample.

To determine the carbon content of the N-Mo_2C/C composite, thermogravimetric analysis (TGA) was performed in air flow from 30 to 700 ℃. Two weight loss districts can be observed in **Fig. S1**, the weight loss (m_1, 98 wt%) originate from the evaporation of adsorbed water below 200 °C; the following stage (m_2, 126 wt%) from 300 to 700 ℃ corresponds to the combustion of surface carbon and the phase transition of MoO_2 to MoO_3. Thus, the content for Mo_2C is (m_2 (wt%)/M(MoO_3)/2×M(Mo_2C))/m_1(wt%) ×100 wt% = 91 wt%. Therefore, the carbon content in the N-Mo_2C/C composite was 9%.

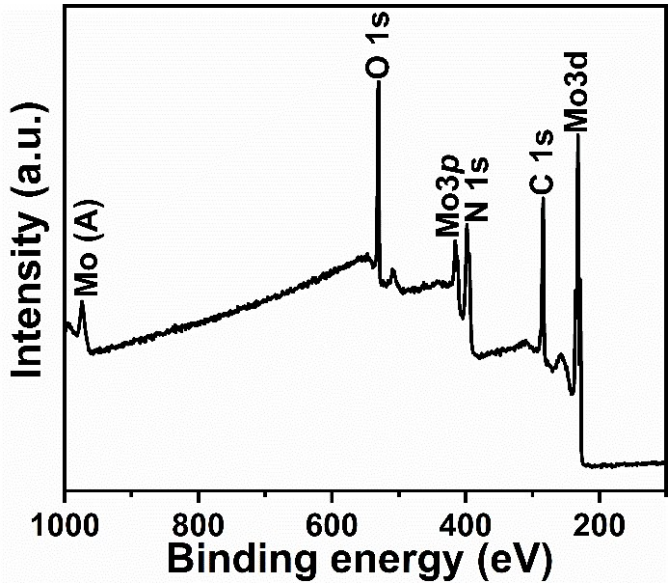

Fig. S2 XPS survey spectrum of N-Mo_2C/C sample consists of Mo 3d, C 1s, N 1s, Mo $3p_{1/2}$, and O 1s species.

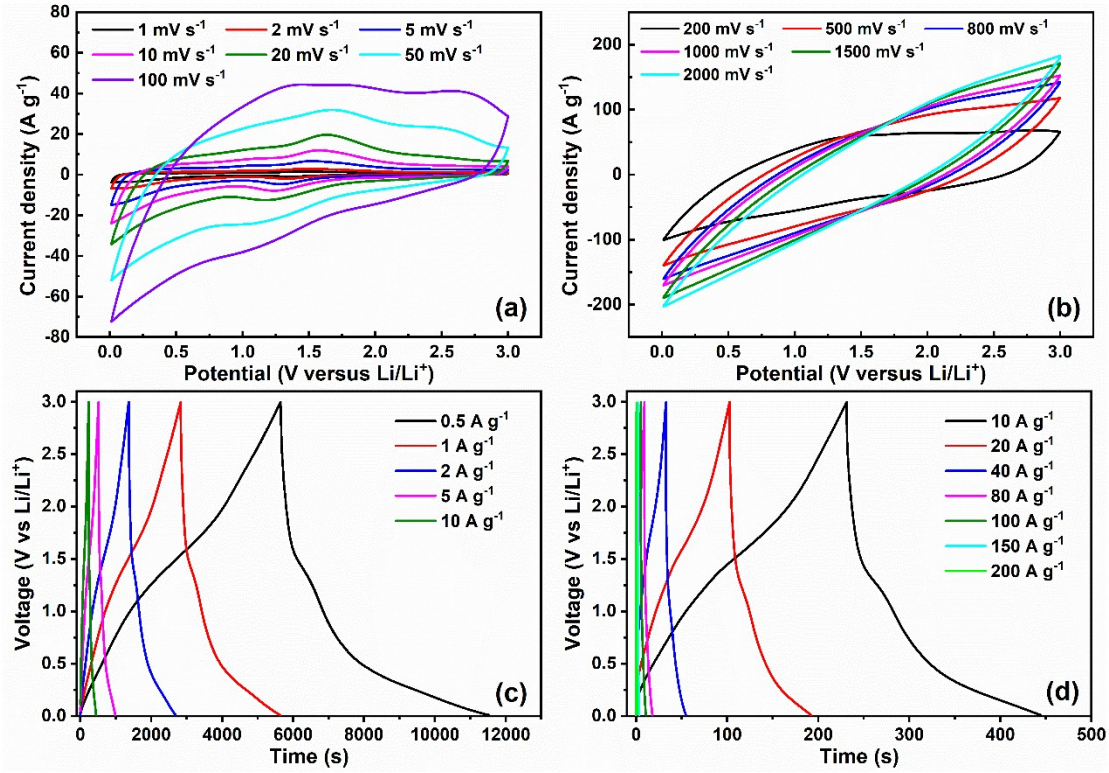

Fig. S3 CV and GCD curves after long-term cycling: (a) and (b) CV curves at different scan rates from 1 to 2000 mV s^{-1}; (c) and (d) GCD curves at different current densities from 0.5 to 200 A g^{-1}.

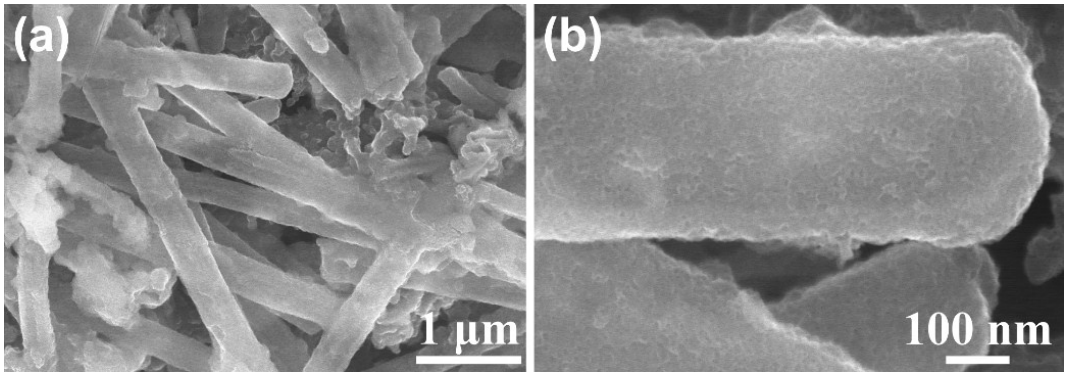

Fig. S4 (a,b) SEM morphology of N-Mo_2C/C nanobelts electrodes after long-term cycling.

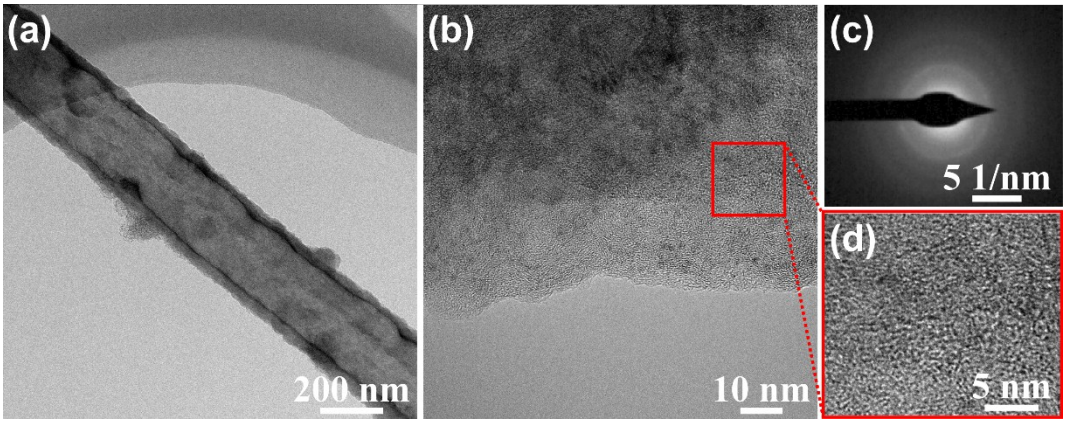

Fig. S5 (a-d) TEM images of N-Mo_2C/C nanobelts electrode after long-term cycling.

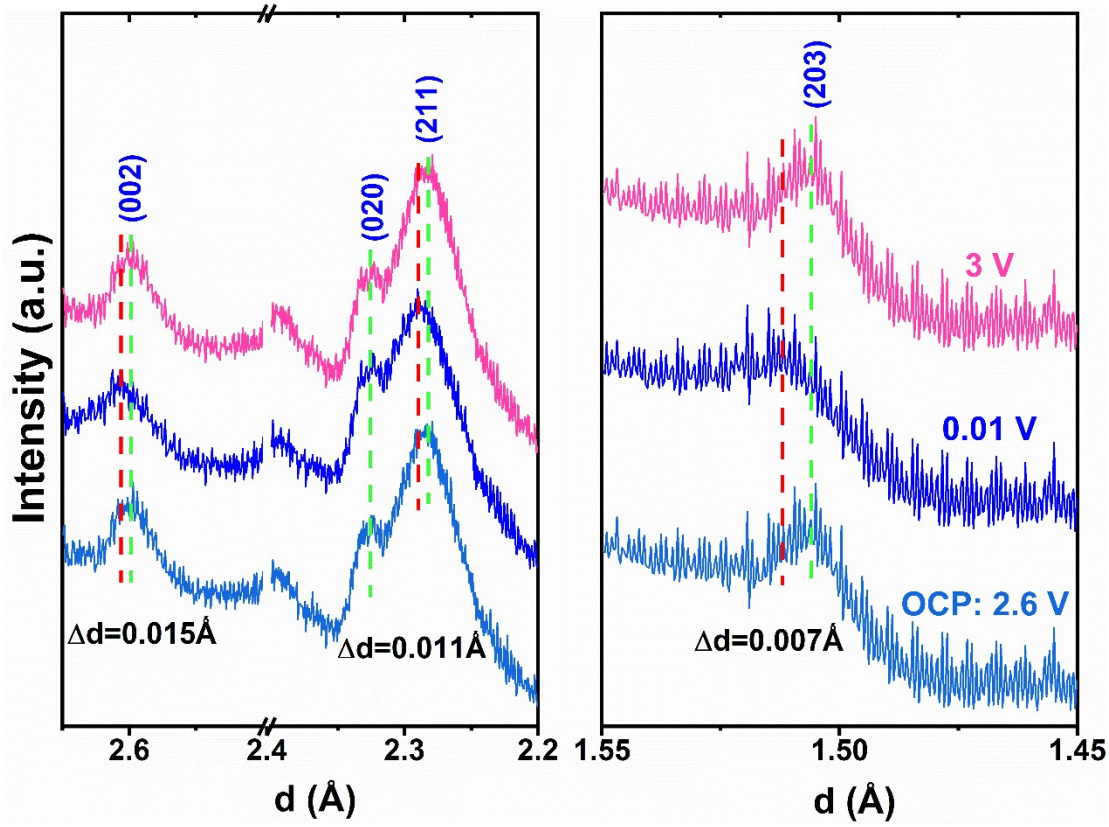

Fig. S6 *Operando* synchrotron XRD patterns of N-Mo_2C/C nanobelts electrode under open circuit voltage, full discharge and charge.

Table S1. Comparison of the electrochemical performances of N-Mo_2C/C with previously reported Mo-based electrodes.

Electrodes	Electrolyte	Capacitance	Current Density / Scan rate	Cycling performance	Ref.
R-MoO_{3-x}	$LiClO_4$	550 C g^{-1}	100 mV s^{-1}	10000 (~76%)	1
GC/MoO_{3-x}	Na_2SO_4	307 C g^{-1}	1 A g^{-1}	-	2
MoO_2/GO	$LiClO_4$	1097 C g^{-1} 390 C g^{-1}	2 mV s^{-1} 1000 mV s^{-1}	10000 (~80%)	3
MoO_2	$LiClO_4$	70 F g^{-1} (63 C g^{-1})	4 A g^{-1}	5000 (~72%)	4
MoS_2@BPC	$NaClO_4$	179.8 mAh g^{-1} (647 C g^{-1})	15 A g^{-1}	5000 (73%)	5
Mo_2C (52.6%)/GR	$LiPF_6$	310 mAh g^{-1} (1116 C g^{-1})	1.6 A g^{-1}	100 (~89%)	6
$Mo_{0.654}C$@CNS	$LiPF_6$	495 mAh g^{-1} (1782 C g^{-1})	5 A g^{-1}	680 (<100%)	7
Mo_2C nanosheets	Na PF_6	85.2 mAh g^{-1} (306.7 C g^{-1})	2 A g^{-1}	1200 (<100%)	8
MnO_2−Mo_2C NFs	Na_2SO_4	302 F g^{-1} (302 C g^{-1})	1 A g^{-1}	5000 (92.6%)	9
Mo_2C/NCF	KOH	1250 F g^{-1} (750 C g^{-1})	1 A g^{-1}	5000 (<100%)	10
$MoSe_2$-Mo_2C	KOH	285 F g^{-1} (285 C g^{-1})	15 A g^{-1}	10000 (98%)	11
N-Mo_2C/C	$LiClO_4$	1139 C g^{-1} 151 C g^{-1} 1166 C g^{-1}	1 mV s^{-1} 2000mV s^{-1} 1 A g^{-1}	15000 (>100%)	**This work**

References

1. H. S. Kim, J. B. Cook, H. Lin, J. S. Ko, S. H. Tolbert, V. Ozolins and B. Dunn, *Nat. Mater.*, 2017, **16**, 454-460.
2. J. Yang, X. Xiao, P. Chen, K. Zhu, K. Cheng, K. Ye, G. Wang, D. Cao and J. Yan, *Nano Energy*, 2019, **58**, 455-465.
3. Y. Zhu, X. Ji, S. Cheng, Z. Y. Chern, J. Jia, L. Yang, H. Luo, J. Yu, X. Peng, J. Wang, W. Zhou and M. Liu, *ACS Nano*, 2019, **13**, 9091-9099.
4. D. V. Pham, R. A. Patil, C.-C. Yang, W.-C. Yeh, Y. Liou and Y.-R. Ma, *Nano Energy*, 2018, **47**, 105-114.
5. Y. Li, H. Wang, B. Huang, L. Wang, R. Wang, B. He, Y. Gong and X. Hu, *J. Mater. Chem. A*, 2018, **6**, 14742-14751.
6. B. Wang, G. Wang and H. Wang, *J. Mater. Chem. A*, 2015, **3**, 17403-17411.
7. J. Zhu, K. Sakaushi, G. Clavel, M. Shalom, M. Antonietti and T. P. Fellinger, *J. Am. Chem. Soc.*, 2015, **137**, 5480-5485.
8. J. Li, Q.-Q. Yang, Y.-X. Hu, M.-C. Liu, C. Lu, H. Zhang, L.-B. Kong, W.-W. Liu, W.-J. Niu, K. Zhao, Y.-C. Wang, F. Cheng, Z. M. Wang and Y.-L. Chueh, *ACS Sustainable Chem. Eng.*, 2019, **7**, 18375-18383.
9. M. Shi, L. Zhao, X. Song, J. Liu, P. Zhang and L. Gao, *ACS Appl. Mater. Interfaces*, 2016, **8**, 32460-32467.
10. K. J. Samdani, D. W. Joh and K. T. Lee, *J. Alloy. Compo.*, 2018, **748**, 134-144.
11. D. Vikraman, S. Hussain, K. Karuppasamy, A. Feroze, A. Kathalingam, A. Sanmugam, S.-H. Chun, J. Jung and H.-S. Kim, *Appl. Catal. B-Environ.*, 2020, **264**, 118531.